Ceramics International 44 (2018) 10790–10796

Contents lists available at ScienceDirect

Ceramics International

journal homepage: www.elsevier.com/locate/ceramint

Annealing temperature influence on sol-gel processed zirconium oxide thin films for electronic applications

Miguel H. Boratto[a,b,*], Mirko Congiu[a], Stevan B.O. dos Santos[a], Luis V.A. Scalvi[a,b]

[a] São Paulo State University (Unesp), School of Sciences, Department of Physics, Bauru, SP 17033-360, Brazil
[b] São Paulo State University (Unesp), School of Sciences, POSMAT – Post-Graduate Program in Materials Science and Technology, Bauru, SP 17033-360, Brazil

ARTICLE INFO

Keywords:
ZrO_2
Dielectric
Annealing effect
Sol-gel

ABSTRACT

A study of zirconium oxide (ZrO_2) thin films obtained by the non-alkoxide sol-gel method at different annealing temperatures, up to 450 °C, is presented. Morphological, compositional, and optical characterizations of zirconia thin films show high transparency and high bandgap, besides homogeneous and non-porous surface. Metal-insulating-metal (MIM) devices were assembled from this zirconia material for electrical characterizations and have shown high electric resistivity and high specific capacitance. A study of the thin film composition shows residues of S and Cl elements from the precursor solution that contributes for reduction of the dielectric constant of the zirconia thin films, even though they still present higher values when compared to SiO_2, which is a positive alternative to replace this oxide in electronic devices. A parallel study of MIM assembled on polymeric substrate and annealed at 100 °C also leads to positive results concerning high electrical insulating and capacitance. This study aims the understanding of the relations between annealing temperature and impurities found in sol-gel based thin films, as well as their relations to dielectric characteristics of zirconia thin films that impact the final properties of electronic devices, such as in field effect transistors.

1. Introduction

Zirconium oxide (ZrO_2) is a ceramic material well known by its hardness, high melting point, and chemical inertness to acid and base solutions. The zirconia ceramics are usually used as refractory materials in furnaces, laser mirrors, ionic conductors, and so on [1]. ZrO_2 thin film has been used within a wide variety of technical and high-temperature applications such as catalysts, fuel cell technology and gas sensor applications [2]. Thus far, it has been one of the most promising oxides for functional and structural materials. Due to properties such as wide bandgap, high refractive index, and low absorption ranging from 240 nm to ~ 8 μm, ZrO_2 thin film is also suitable for use as active-waveguide sensors and coatings of optical filters in ultraviolet to infrared spectral region [2–5].

In order to find a substitute for the well-established silicon dioxide (SiO_2) in metal-oxide-semiconductor field-effect transistors (MOSFETs) [6], dielectric oxides with high dielectric constant (high-*k*) have been investigated, such as hafnia (HfO_2), alumina (Al_2O_3), and zirconia (ZrO_2), because they are suitable to improve the channel modulation in MOSFETs through reduced tunneling current, even for small thicknesses [7–9]. Zirconia is a favorable alternative due to its high dielectric constant (k = 18–26), wide bandgap (4.7–7.8 eV), good thermal stability against silicate formation, excellent chemical inertness, high breakdown field, and good catalytic properties [2,3,10,11].

For application in electronics, ZrO_2 thin film are obtained by costly methods at temperatures higher than 500 °C [12], such as high vacuum methods, including reactive sputtering, atomic layer deposition (ALD) [4,10], electron beam evaporation [13], oxidation of Zr metal film by thermo-oxidation or ultraviolet ozone [3], and pulsed layer deposition. The approach of sol-gel deposition for ZrO_2 thin films offers besides the reduced cost, significant technical/application advantages, such as the simple and fast fabrication process [2]. The preparation of ZrO_2 thin films at low temperature remains challenging, and in order to decrease the process temperature to make possible the fabrication of zirconia thin films on both glass and plastic substrates, many approaches have been proposed [12,14–17]. The non-alkoxide route is well known for obtaining porous films [18] and powders [19], though, non-porous films were obtained by Rizzato and collaborators [20]. In this work we present the investigation and finding of homogeneous, non-porous, and high electrical insulating ZrO_2 thin films deposited by non-alkoxide sol-gel route at different processing temperatures. The morphological, optical and electrical properties of the zirconia thin films are investigated in order to employ this insulating layer in future electronic applications, such as memristor [5,21,22] and transistor devices [5,6]. In this paper,

* Corresponding author at: São Paulo State University (Unesp), School of Sciences, Department of Physics, Bauru, SP 17033-360, Brazil.
E-mail address: miguel@fc.unesp.br (M.H. Boratto).

https://doi.org/10.1016/j.ceramint.2018.03.117
Received 28 January 2018; Received in revised form 13 March 2018; Accepted 13 March 2018
Available online 14 March 2018

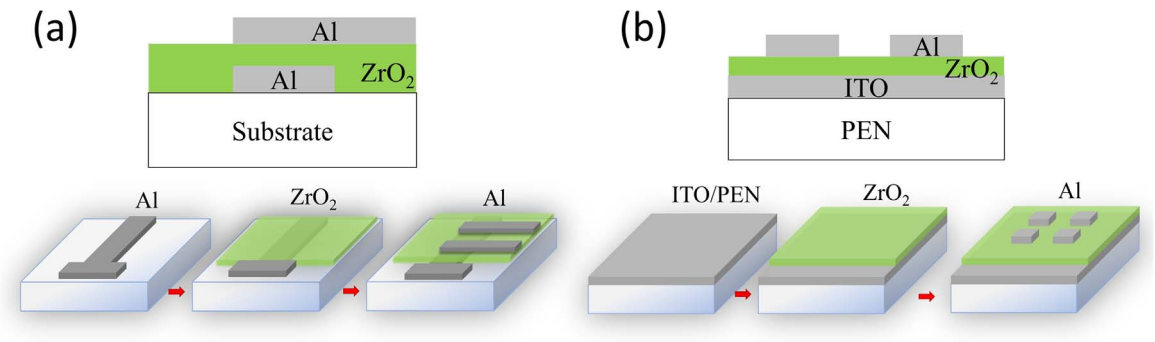

Fig. 1. Steps to obtain the zirconia thin film based metal-insulator-metal capacitor for vertical electrical characterization on **(a)** glass substrate, and on **(b)** ITO/PEN substrate.

an extensive study of ZrO_2 thin films deposited on different substrates at different annealing temperatures is presented, as well as its dielectric performance obtained through electrical characterizations on metal-insulator-metal (MIM) capacitors.

2. Methodology

The stable ZrO_2 solution was obtained through the method proposed by Chiavacci and coworkers [18], by using zirconyl chloride ($ZrOCl_2{\cdot}8H_2O$) precursor dissolved in hydrochloric acid (HCl), which was added dropwise to a warm (80 °C) solution of sulfuric acid (H_2SO_4) at 0.21 M, in a molar ratio of Zr^{4+}:H_2SO_4 of 3:1, producing a final volume of 500 mL, at concentration of 0.2 M. After dialysis against distilled water, the colloidal suspension reaches pH 1.6 and concentration of 0.1 M [16,20]. To increase the viscosity, 100 mL of the solution was concentrated at 98 °C until reach a final volume of 10 mL (1.0 M). The concentrated solution was used for thin film deposition without any Supplementary step.

Zirconia powder was obtained by completely evaporating the solution at 98 °C. The as-obtained material was used for thermal characterization (TGA/DSC) and structural analysis (XRD) yielding information about phase changes, mass losses and the crystalline structure. Thermal Gravimetric Analysis (TGA) and Differential Scanning Calorimetry (DSC) were carried out using a STA 409 (Netzsch) with a rate of 10 °C/min from 50 °C to 1200 °C in a controlled N_2 atmosphere. The powders annealed at 1000 °C for 1 h were investigated through X-Ray Diffraction (XRD) in a Rigaku DMAX diffractometer with CuKα beam, Ni filter, at 2θ/θ scan from 10° to 80°.

Substrates of quartz, glass, indium tin oxide coated polyethylene naphthalate (ITO/PEN) and Si/SiO_2 were cleaned by a mixture of water and detergent, followed by isopropyl alcohol prior to thin film depositions. Two methods of deposition were used: spin-coating at 3000 rpm for 1 min, and dip-coating at 10 cm/min. Different temperatures of intermediary and final thermal annealing, from 100 °C to 450 °C, were also performed on the samples in order to eliminate the organic and solvent residues in the route to obtain the ZrO_2 film. Soo and collaborators [2] report that coated substrates baked under infrared lamp followed by annealing at 450 °C resulted in amorphous ZrO_2, although most of the literature reports that at thermal annealing higher than 400 °C the amorphous zirconia changes to metastable tetragonal phase (t-ZrO_2).

The deposition of 4 layers of ZrO_2 on Si/SiO_2 occurred by spin-coating of the concentrated zirconia solution (1.0 M) at 3000 rpm, followed by thermal annealing after the deposition of the last layer. These samples were used for Rutherford Backscattering (RBS) and Atomic Force Microscopy (AFM) characterizations, in order to study the films composition and morphology, aiming verifying the concentration and elimination of solvent residues from the precursor solution in the films. The RBS measurement was performed at the Western University Tandetron Accelerator facility, using the $^4He^{2+}$ beam with 2.5 MeV, and a silicon barrier detector in Cornell geometry at an angle of 170°. The data analysis was done with SIMNRA software. The AFM analysis was performed in a Witec GmbH, model Alpha 300 S.

ZrO_2 thin films deposited on quartz substrate were used for UV–Vis–NIR transmittance, that was carried out in a spectrophotometer Varian Inc, model DMS 80, in order to investigate its transparency on the UV–Vis–NIR spectra, and to allow bandgap evaluation. Deposition of zirconia thin films on glass substrate by dip-coating followed by thermal annealing at 450 °C for 1 h, was also investigated through XRD with 2θ scan and 1.5° incident angle.

The assembly of devices based on ZrO_2 film was done on glass and ITO/PEN substrates to perform electrical characterization for evaluation of the dielectric layer. A simplified diagram to obtain the employed devices is presented in Fig. 1, as well as their obtaining steps. Firstly, it was evaporated a bottom aluminum electrode on the glass substrate, followed by the deposition of two layers of ZrO_2 thin film by dip-coating. Intermediary and final thermal annealing were performed at 450 °C after the deposition of the first layer, for 10 min, and after the second layer, for 60 min. The same deposition occurred on the ITO/PEN substrate at intermediary and final annealing temperature of 100 °C. On this substrate the ITO layer acts as bottom electrode. Top Al electrodes were then evaporated to complete the device. Electrical measurements were performed through Cyclic Voltammetry (CV), and Impedance Spectroscopy (IS) in a Metrohm AutoLab PGSTAT302 equipped with FRA32M module.

3. Results

3.1. ZrO_2 thin films

A preliminary study was performed to define the suspension concentration to be used to deposit the zirconia thin films. Concentrations of 0.4 M and 1.0 M were tested, and the higher concentration of the sol-gel suspension revealed to produce more uniform films, with less pores compared to the solution 0.4 M. Consequently, the zirconia layers were obtained from suspension with 1 M concentration.

The optical characterization of two layers of the zirconia spin-coated on quartz substrate resulted in the UV–vis transmittance and bandgap obtained through Tauc's plot [23] shown in Fig. 2. The zirconia film presents high transparency in the visible region spectra and a direct bandgap E_G = 5.8 eV, in good agreement with published values [11,24].

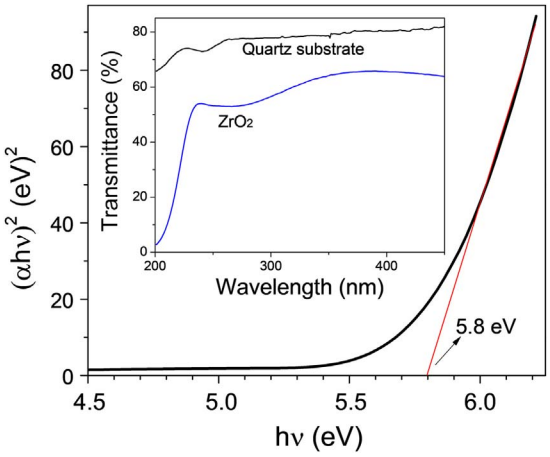

Fig. 2. Tauc plot of the ZrO_2 film on quartz substrate. Inset: Transmittance in the UV–vis spectra.

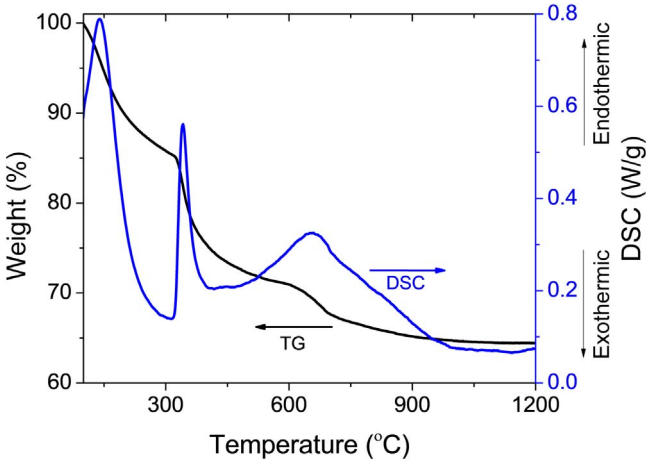

Fig. 4. TG/DSC curves of the powder of ZrO_2.

The diffractogram of zirconia thin films, dip-coated on glass substrates and annealed at 450 °C is presented in Fig. 3(a). When grown by spin-coating the diffractogram is very similar, and in these conditions, the film presents an amorphous structure without any characteristic peak related to any ZrO_2 known phase. On the other hand, when the powder sample is annealed at 1000 °C for 1 h one can notice a fair crystalline structure, as observed in Fig. 3(b), presenting characteristic peaks of monoclinic ZrO_2 (JCPDS 100-8297).

In order to understand the processes occurring during the sample annealing, TGA/DSC measurements were performed on powder samples. This analysis was compulsory to verify the temperature-induced mass loss (i.e. release of ionic compounds of the precursor solution), as well as different thermal processes (endo/exothermal) occurring during the material heating. The results are shown in Fig. 4, where it is possible to notice a mass loss up to 15% from 100 to 350°C, probably due to the elimination of adsorbed water and hydroxyl groups attached to zirconia (ZrO_2-OH) in the range 150–250 °C, and Cl_2 in the range of 300–400 °C [20]. From 350 to 700°C another significant mass loss (~ 15%) is noticeable probably due to the loss of SO_4 as also reported in literature [20]. Up to 350 °C the density of the solid remains the same through the volume reduction that follows the mass reduction, although, the density decreases above 350 °C probably as consequence of the increase of porosity due to gaseous species evolution related to Cl_2, ClO_X, S, and SO_X compounds [20].

The DSC curve shows endothermic peaks at 142 °C and 342 °C that may be related to the temperatures that start to promote the liberation of Cl_2 and SO_4. The endothermic peak at 655 °C is probably related to the phase-transition from metastable tetragonal to monoclinic. This monoclinic structure of the zirconia annealed at 1000 °C is also observed in the XRD data (Fig. 3b). An overall mass loss of approximately 35 wt% is achieved until the end of the temperature ramp.

To verify the surface homogeneity and composition of the thin films obtained from the non-alkoxide method and compare with the results presented by TG/DSC, the suspension 1 M was used to deposit thin films on Si/SiO_2 substrates with a total of 4 layers spin-coated without intermediate calcination, but with final thermal annealing in the temperature range of 250–450 °C for 1 h. The samples were characterized by Rutherford Backscattering Spectrometry (RBS) and the data were analyzed through simulation using the SIMNRA software [21]. The Fig. 5(a) shows the RBS data, experimental and simulated, of ZrO_2 film thermal annealed at 450 °C after deposition of the last layer. One can verify through the continuous experimental curve that the thin film is homogeneous and regular, without noticeable porosity. It is also observed the presence of some impurities such as the elements Hf, S, Cl, within the ZrO_2 film, as well as Si and O from the Si/SiO_2 substrate. The existence of hafnium at concentration of 0.5% is due to its presence as impurity in the $ZrOCl_2{\cdot}8H_2O$ precursor used to produce the sol-gel suspension. The residual presence of Cl and S from the precursor solution is mostly due to the zirconia film deposition of four layers, which are annealed at 450 °C only after the last one has been deposited. The total removal of Cl_2 and SO_4 at 350 °C and 500 °C [20] are not achieved due to superficial elimination, and subsequently, trapping of these

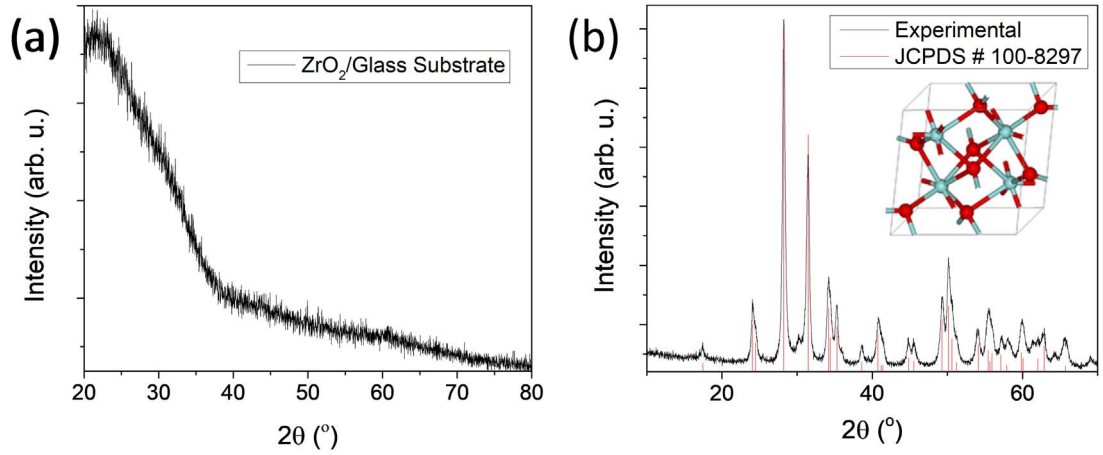

Fig. 3. Diffractogram of zirconia **(a)** thin film and **(b)** powder after 1 h of thermal annealing at 450 °C and 1000 °C, respectively. Inset of (b): ZrO_2 monoclinic structure, where Zr atoms are represented in red, and O atoms are represented in blue. (For interpretation of the references to color in this figure legend, the reader is referred to the web version of this article.)

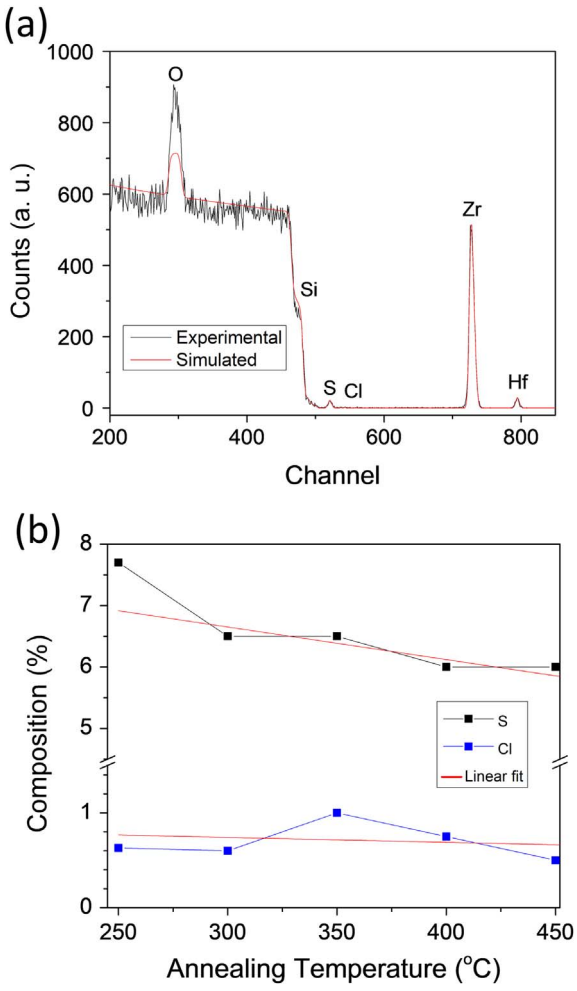

Fig. 5. (a) RBS experimental and simulated data of the ZrO_2 spin-coated on SiO_2/Si substrate. **(b)** Concentration of S and Cl within the ZrO_2 films as function of the annealing temperature.

elements within the first layers. Fig. 5(b) shows the dependence of the annealing temperature to eliminate the S and Cl. The initial atomic concentrations of S and Cl in the films with thermal annealing at 250 °C are 7% and 0.8%, respectively. After increase in annealing temperature (up to 450 °C) the concentration of S reduces to 5.5% and Cl reduces to 0.6%, following a linear reduction as function of the temperature, totalizing 21% and 25% of specific reduction of S and Cl, respectively. Once more, the considerable concentration of these elements is due to their incorporation within the first deposited layers with no thermal annealing.

AFM was also performed on the zirconia film with thermal annealing at 450 °C, previously characterized by RBS, for morphological analysis, as shown in Fig. 6(a). The image presents a homogeneous and non-porous surface, reinforcing the findings of RBS measurements. Fig. 6(b) shows a higher magnification of the surface, which is clearly granular. The inset presents the surface cross-section profile that shows the smooth and low roughness surface.

3.2. ZrO_2 applied to MIM devices

3.2.1. Zirconia based MIMs on glass substrates

After an inspection on the optical, structural, compositional, and morphological characteristics of the ZrO_2 obtained by the non-alkoxide method, the electrical characterization of the ZrO_2 based devices shown in Fig. 1 were performed to verify the effects of the presence of impurities within the zirconia films on the overall electric characteristics of the dielectric layer. As presented by RBS results, the presence of impurities within the zirconia films is mostly related to absence of thermal calcination between layers, thus, in the proposed devices the dielectric thin film is formed by only two layers of ZrO_2 deposited by dip-coating, with 10 min of calcination and 60 min of annealing after the first and second layers, respectively, both at 450 °C. Al electrodes were evaporated after the zirconia deposition to complete the metal-insulator-metal (MIM) device assembly. Although the attempt to eliminate the impurities has occurred, the ZrO_2 films annealed at 450 °C after each layer also present small concentration of S and Cl elements, as shown by energy dispersive X-ray spectroscopy (EDS) results (Supplementary information, Fig. S1).

A topographic characterization of ZrO_2 thin films deposited by dip-coating on glass substrate was performed through confocal microscopy using a Leica DCM 3D microscope. A root mean square roughness of

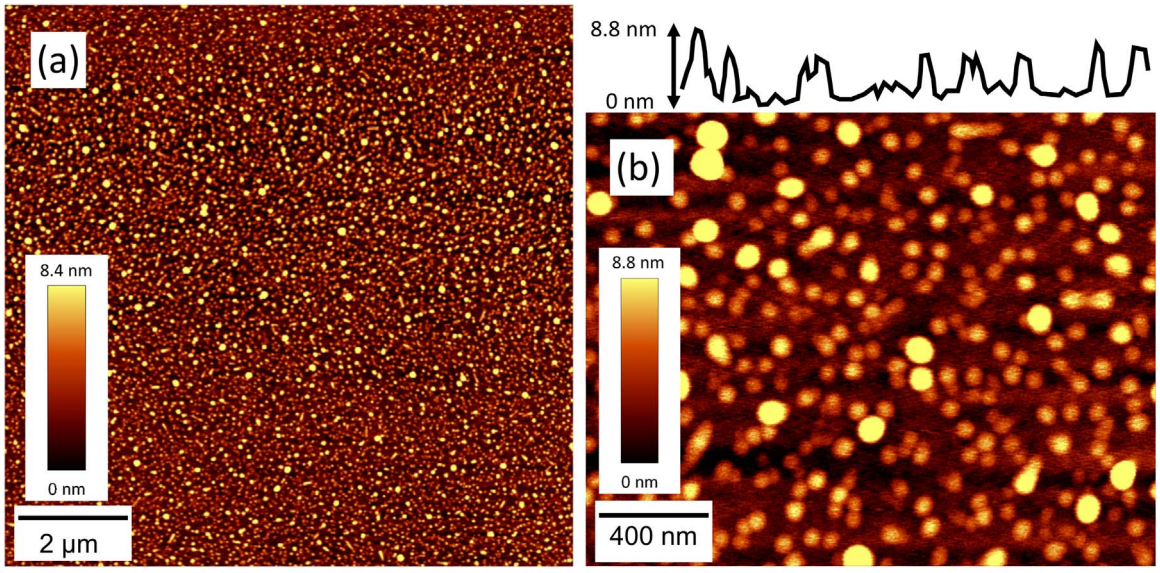

Fig. 6. (a) Atomic Force Microscopy of the $ZrO_2/SiO_2/Si$ deposited by spin-coating at 3000 rpm. **(b)** Higher magnification image that shows similar topography and details of the grains on the surface. Inset: Surface cross-section profile.

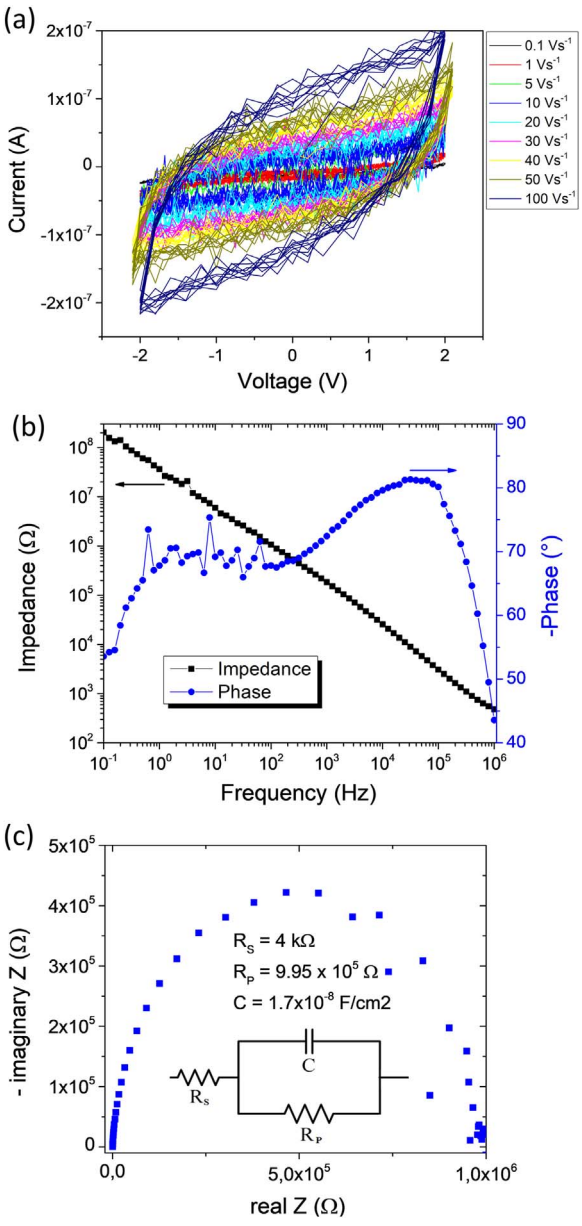

Fig. 7. (a) Cyclic Voltammetry at scan rate voltages from 100 mV s^{-1} to 100 V s^{-1}, performed on MIM devices shown in Fig. 1(a). A total of 5 cycles is presented for each curve. **(b)** Bode plot with Impedance and Phase as function of operation frequency. **(c)** Nyquist plot of the ZrO_2 based MIM device in parallel with a $R_P = 9.9 \times 10^5$ Ω commercial resistor. (For interpretation of the references to color in this figure, the reader is referred to the web version of this article.)

40 nm (Fig. S2a), and film thickness of about 200 nm (Fig. S2b) were obtained for films deposited through the solution concentrated at 1.0 M. This dip-coating deposition method became the standard deposition for the samples electrically characterized, thus the zirconia film thickness presented here is considered in the calculations of dielectric constants.

The electrical measurements took place at room temperature and pressure. The Fig. 7(a) presents the results obtained from cyclic voltammetry at several triangular-wave voltage scan rates. One can see that at faster scan rates the electrical resistance is reduced from $R = 5 \times 10^8$ Ω to $R = 1 \times 10^7$ Ω, at 0.1 and 100 V s^{-1}, respectively. Moreover, an increase in capacitive characteristic arises from the hysteresis of the current curve, that represents the charge loading in the Al electrodes. In order to better evaluate the electrical impedance of the zirconia based MIM devices, the impedance results are presented through the black curve in Fig. 7(b). As previously seen in Fig. 7(a), the maximum impedance $Z = 2 \times 10^8$ Ω obtained at 0.1 Hz, in Fig. 7(b), is reduced to $Z = 5 \times 10^2$ Ω at 1 MHz. The resistivity (ρ) was calculated considering the electrical resistance at DC voltage ($R = 5 \times 10^8$ Ω) through equation $\rho = R.A/L$, where L is the distance between contacts, in this case the film thickness $L = 200$ nm (Supplementary information, Fig. S2), and A is the conduction cross section area, between contacts, $A = 0.04$ cm^2. A high resistivity $\rho = 9.9 \times 10^9$ Ω m was found, in good agreement with reported values [25].

The capacitive characteristic of the zirconia thin film was further investigated, leading to results presented in Fig. 7(b) and (c). The current-voltage phase difference (blue curve) is presented in Fig. 7(b), where it is possible to verify that the phase presents values higher than − 60° from 1 Hz through 10^5 Hz, with a maximum at − 80°, close to a perfect capacitor that would present − 90° phase. The Nyquist plot presented in Fig. 7(c) was performed with a $R_P = 9.9 \times 10^5$ Ω commercial resistor in a parallel configuration with a zirconia based MIM device working as a capacitor in the circuit, as shown in the inset of Fig. 7(c). The result shows that the MIM device presents a relatively high specific capacitance of about 1.7×10^{-8} F/cm^2. The dielectric constant (k) of the zirconia thin film within the capacitor was obtained through the average values of capacitance $C = 3.7 \times 10^{-8}$ F/cm^2, and the maximum value found was $k = 8.5$, which is smaller than values reported for zirconia (k = 18–23) [2,3]. Although this result is not the state-of-the-art, it is still greater than SiO_2 dielectric constant ($k = 3.9$) [3,7] which is a positive characteristic and indicates a possibility of application of this ZrO_2 deposited by sol-gel for replacement of the silicon oxide in field-effect transistor devices.

The dielectric loss, present in our samples at high frequencies, can be related to the delay of molecular polarization with respect to the alternating electric field inside the capacitor due to the existence of impurity ions in the dielectric layer that may increase the dipole and ionic relaxations, which weakens the dipole formation in the dielectric film.

3.2.2. Zirconia based MIMs on polymeric substrates

ZrO_2 thin films were also obtained at low temperature (T = 100 °C) on ITO coated polyethylene naphthalate (PEN) polymeric substrates (ZrO_2/ITO/PEN), as shown in Fig. 8(a). The same deposition method previously described for ZrO_2/Al/glass samples was done in these samples, although, the intermediary and final thermal annealing were performed at 100 °C for 20 and 60 min, respectively. Such low temperature was used to not damage both the ITO conductive properties and the polymeric substrate. Electrical characteristics of these MIM devices were also evaluated to verify the thermal annealing and ITO electrode effects in such devices. As seen in TG/DSC and RBS results of Figs. 4 and 5, samples with lower thermal annealing temperature tends to present higher concentrations of S and Cl elements, which impact considerably the dielectric performance and capacitance of these devices.

Bode and capacitance plots are presented in Fig. 8(b). Even though the annealing temperature is low, the samples still present impedance as high as $Z = 2 \times 10^8$ Ω at low frequencies, the same value found for samples with higher annealing temperature on glass substrate. The capacitance obtained in these devices are $C = 3 \times 10^{-10}$ F/cm^2 and $C = 3 \times 10^{-9}$ F/cm^2 at frequencies of 10^6 and 10^1 Hz, respectively (Fig. S3). The lower maximum capacitance (3×10^{-9} F/cm^2) found in these devices compared to ones of previously investigated devices assembled on glass substrates (Section 3.2.1), may be related mostly to the larger quantity of impurities rather than the different electrodes (ITO/Al) of devices deposited on polymeric substrate.

The current-voltage phase difference presents high variation in samples on polymeric substrate compared to devices annealed at 450 °C on glass substrate. The ZrO_2/ITO/PEN presents more resistive characteristic, with phase closer to 0, at low frequencies ($< 10^3$ Hz) compared to samples on glass substrate that preserves high phase angle in that low frequency range. Such difference may occur due to higher

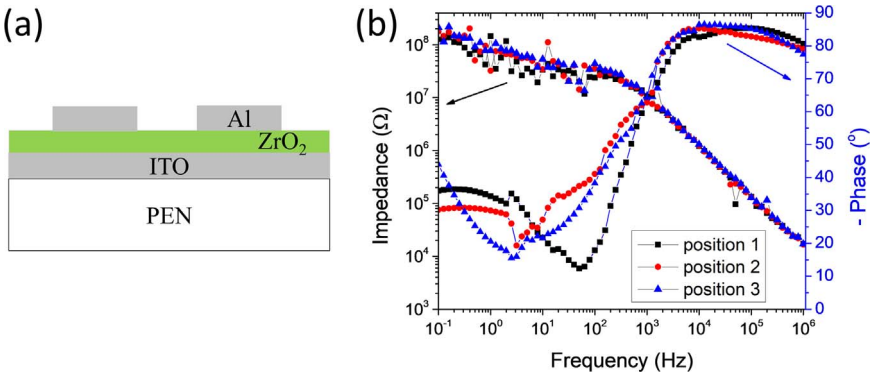

Fig. 8. (a) ZrO_2 thin film based MIM devices on flexible substrate and annealing at 100 °C with square Al electrodes (A = 0.04 cm^2). **(b)** Bode plot of Impedance *vs* frequency (left axis), and phase *vs* frequency (right axis). Measurements were performed in different Al electrode positions.

concentration of impurity components and its consequently higher disorder within the zirconia layer annealed at 100 °C. The resistive characteristic preserves the high impedance at higher frequencies. For example, the impedance of samples annealed at 450 °C decreases to $Z = 10^6$ Ω (200 times lower) at 10^2 Hz, while the impedance of polymeric samples decreases to $Z = 3 \times 10^7$ Ω (7 times lower) at the same frequency. The higher impedance found in ZrO_2/ITO/PEN samples may be related to the higher work function (4.7 eV) of the ITO electrode [26] that increases the ZrO_2/ITO conduction band discontinuity [27] decreasing the carrier injection and the leakage current.

The different concentrations of impurity elements originated from the precursor solution has shown strong effect in the capacitive and resistive characteristics of the dielectric thin films. The insulating characteristics of the ZrO_2 thin films obtained by sol-gel method concern the very different annealing temperatures and distinct substrates, producing distinct devices with competitive properties and performance similar to ones based on SiO_2.

4. Conclusion

This work presents the analysis of ZrO_2 thin films obtained by non-alkoxide sol-gel method at different annealing temperatures. The results reported here show the relation between annealing temperature and impurities found in sol-gel zirconia thin films as well as their relationship with the capacitive characteristic of the dielectric layer, which is a fundamental property for specific electronic applications and at specific frequency operations, such as in field effect transistors (FET). Zirconia thin films annealed at 450 °C have presented high transparency, homogeneous and non-porous surface, and optical bandgap of 5.8 eV, within values reported in literature. The study of the thin film composition showed residues of S and Cl elements from the precursor solution that contribute for the reduced dielectric constant of the zirconia thin films through the increase of dipole and ionic relaxations, that deteriorates the dipole formation in the dielectric film. Even though a lower dielectric constant was found due to such impurities, it is still higher than SiO_2 dielectric constant, which indicates a possibility of application of the ZrO_2 deposited by sol-gel for replacement of the latter oxide in electronic devices. In addition, MIM devices on glass and polymeric substrates presented high electric resistivity and specific capacitance, even at annealing temperature as low as 100 °C. Both findings are indispensable characteristics for applications as insulating dielectric layer in electronics, and specifically in FETs. In summary, this work shows that lower annealing temperature contributes to higher impurity concentration within the ZrO_2 film, which depreciates its dielectric characteristics. However, all the results shown in this communication suggest that zirconium oxide obtained through non-alkoxide sol-gel method presents competitive characteristics for application in capacitors and transistors.

Acknowledgements

We would like to thank professors G. Fanchini and L.V. Goncharova for valuable discussions at University of Western Ontario, Canada. We also acknowledge Professor C.V. Santilli and Dr. M.A. Rosa from Chemistry Institute (UNESP – Araraquara-SP) for help with ZrO_2 solution processing, and Professor C.F.O. Graeff for AutoLab equipment. We thank the financial support from CAPES, CNPq, and FAPESP (Grants 16/16423-6 and 16/17302-8).

Appendix A. Supplementary material

Supplementary data associated with this article can be found in the online version at http://dx.doi.org/10.1016/j.ceramint.2018.03.117.

References

[1] D.F. Maia, D.A. Costa, A.C.F.M. Costa, L. Gama, H.L. Lira, Morphological Aspects of Zirconia from Pechini Method, 2000.
[2] M.T. Soo, N. Prastomo, A. Matsuda, G. Kawamura, H. Muto, A.F.M. Noor, Z. Lockman, K.Y. Cheong, Elaboration and characterization of sol-gel derived ZrO 2 thin films treated with hot water, Appl. Surf. Sci. 258 (2012) 5250–5258, http://dx.doi.org/10.1016/j.apsusc.2012.02.008.
[3] Y. Dora, S. Han, D. Klenov, P.J. Hansen, K. No, U.K. Mishra, S. Stemmer, J.S. Speck, ZrO2 gate dielectrics produced by ultraviolet ozone oxidation for GaN and AlGaN/GaN transistors, J. Vac. Sci. Technol. B Microelectron. Nanometer. Struct. 24 (2006) 575, http://dx.doi.org/10.1116/1.2167991.
[4] A. Javey, H. Kim, M. Brink, Q. Wang, A. Ural, J. Guo, P. McIntyre, P. McEuen, M. Lundstrom, H. Dai, High-kappa dielectrics for advanced carbon-nanotube transistors and logic gates, Nat. Mater. 1 (2002) 241–246, http://dx.doi.org/10.1038/nmat769.
[5] D. Panda, T.-Y. Tseng, Growth, dielectric properties, and memory device applications of ZrO2 thin films, Thin Solid Films 531 (2013) 1–20, http://dx.doi.org/10.1016/j.tsf.2013.01.004.
[6] M.H. Boratto, L.V.A. Scalvi, L.V. Goncharova, G. Fanchini, Effects of solution history on sol-gel processed tin-oxide thin-film transistors, J. Am. Ceram. Soc. 99 (2016) 4000–4006, http://dx.doi.org/10.1111/jace.14459.
[7] M.H. Boratto, L.V.A. Scalvi, Deposition of Al2O3 by resistive evaporation and thermal oxidation of Al to be applied as a transparent FET insulating layer, Ceram. Int. 40 (2014) 3785–3791, http://dx.doi.org/10.1016/j.ceramint.2013.09.041.
[8] M.H. Boratto, L.V.A. Scalvi, J.L.B. Maciel Jr, M.J. Saeki, E.A. Floriano, Heterojunction between Al2O3 and SnO2 thin films for application in transparent FET, Mater. Res. 17 (2014) 1420–1426, http://dx.doi.org/10.1590/1516-1439.285114.
[9] N. Padmamalini, K. Ambujam, Structural, dielectric and impedance studies on high-k ZrO2-TiO2 nanocomposite, J. Mater. Sci. Mater. Electron. 28 (2017) 4690–4694, http://dx.doi.org/10.1007/s10854-016-6109-6.
[10] G. Ye, H. Wang, S. Arulkumaran, G.I. Ng, R. Hofstetter, Y. Li, M.J. Anand, K.S. Ang, Y.K.T. Maung, S.C. Foo, Atomic layer deposition of ZrO2 as gate dielectrics for AlGaN/GaN metal-insulator-semiconductor high electron mobility transistors on silicon, Appl. Phys. Lett. 103 (2013) 2011–2014, http://dx.doi.org/10.1063/1.4824445.
[11] D. Xiao, G. He, Z. Sun, J. Lv, P. Jin, C. Zheng, M. Liu, Microstructure, optical and electrical properties of solution-derived peroxo-zirconium oxide gate dielectrics for CMOS application, Ceram. Int. 42 (2015) 759–766, http://dx.doi.org/10.1016/j.ceramint.2015.08.177.
[12] Y. Mi, J. Wang, Z. Yang, Z. Wang, H. Wang, S. Yang, A simple one-step solution deposition process for constructing high-performance amorphous zirconium oxide thin film, RSC Adv. 4 (2014) 6060–6067, http://dx.doi.org/10.1039/c3ra46169f.

[13] H. Fukumoto, M. Morita, Y. Osaka, Electrical characteristics of metal-insulator-semiconductor diodes with ZrO_2/SiO_2 dielectric films, J. Appl. Phys. 65 (1989) 5210–5212, http://dx.doi.org/10.1063/1.343155.
[14] C. Avis, J. Jang, High-performance solution processed oxide TFT with aluminum oxide gate dielectric fabricated by a sol–gel method, J. Mater. Chem. 21 (2011) 10649, http://dx.doi.org/10.1039/c1jm12227d.
[15] K.K. Banger, Y. Yamashita, K. Mori, R.L. Peterson, T. Leedham, J. Rickard, H. Sirringhaus, Low-temperature, high-performance solution-processed metal oxide thin-film transistors formed by a “sol–gel on chip” process, Nat. Mater. 10 (2011) 45–50, http://dx.doi.org/10.1038/nmat2914.
[16] J. Livage, F. Beteille, C. Roux, M. Chatry, P. Davidson, Sol - gel synthesis of oxide materials, Acta Mater. 46 (1998) 743–750.
[17] J.J. Yu, I.W. Boyd, ZrO2 films deposited by photo-CVD at low temperatures, Appl. Phys. A Mater. Sci. Process. 75 (2002) 489–491, http://dx.doi.org/10.1007/s003390201294.
[18] L.A. Chiavacci, S.H. Pulcinelli, C.V. Santilli, V. Briois, Structural and phenomenological characterization of the thermoreversible sol-gel transition of a zirconyl aqueous precursor modified by sulfuric acid, Chem. Mater. 10 (1998) 986–993, http://dx.doi.org/10.1021/cm970387d.
[19] A. Majedi, A. Abbasi, F. Davar, Green synthesis of zirconia nanoparticles using the modified Pechini method and characterization of its optical and electrical properties, J. Sol-Gel Sci. Technol. 77 (2016) 542–552, http://dx.doi.org/10.1007/s10971-015-3881-3.
[20] A.P. Rizzato, C.V. Santilli, S.H. Pulcinelli, X-ray reflectivity of zirconia based sol-gel coatings on borosilicate glasses, J. Non Cryst. Solids 247 (1999) 158–163.
[21] M.H. Boratto, R.A. Ramos Jr, M. Congiu, C.F.O. Graeff, L.V.A. Scalvi, Memristive behavior of the SnO2/TiO2 interface deposited by sol-gel, Appl. Surf. Sci. 410 (2017) 278–281, http://dx.doi.org/10.1016/j.apsusc.2017.03.132.
[22] H. Zhang, B. Gao, B. Sun, G. Chen, L. Zeng, L. Liu, X. Liu, J. Lu, R. Han, J. Kang, B. Yu, Ionic doping effect in ZrO2 resistive switching memory, Appl. Phys. Lett. 96 (2010) 123502, http://dx.doi.org/10.1063/1.3364130.
[23] J. Tauc, Optical properties and electronic structure of amorphous Ge and Si, Mater. Res. Bull. 3 (1) (1968) 37–46.
[24] G. Adamopoulos, S. Thomas, P.H. Wöbkenberg, D.D.C. Bradley, M.A. McLachlan, T.D. Anthopoulos, High-mobility low-voltage ZnO and Li-doped ZnO transistors based on ZrO2 high-k dielectric grown by spray pyrolysis in ambient air, Adv. Mater. 23 (2011) 1894–1898, http://dx.doi.org/10.1002/adma.201003935.
[25] S.K. Tadokoro, E.N.S. Muccillo, Zircônia tetragonal policristalina. Parte II: Microestrutura e resistividade elétrica, Cerâmica 47 (2001).
[26] C. Sun, X. Li, G. Wang, P. Li, W. Zhang, T. Jiu, N. Jiang, J. Fang, Highly efficient inverted polymer solar cells using fullerene derivative modified TiO2 nanorods as the buffer layer, RSC Adv. 4 (2014) 19529, http://dx.doi.org/10.1039/c4ra02254h.
[27] K.C. Chiang, C.H. Cheng, K.Y. Jhou, H.C. Pan, C.N. Hsiao, C.P. Chou, S.P. McAlister, A. Chin, H.L. Hwang, Use of a high-work-function Ni electrode to improve the stress reliability of analog SrTiO3 metal-insulator-metal capacitors, IEEE Electron Device Lett. 28 (2007) 694–696, http://dx.doi.org/10.1109/LED.2007.900876.